

# Reliability of Stereo Vision and Vicon Motion Capture Systems for Measurement of Interfragmentary Movements

CV Mwenecho<sup>a</sup>, AD Indekeu<sup>b</sup>, N Ferreira<sup>c</sup>, O Bergh<sup>d</sup>, K Schreve<sup>e</sup>

Received 26 March 2025, in revised form 16 September 2025 and accepted 2 December 2025

**Abstract:** *Interfragmentary movement (IFM) of bone fragments in an external fixator is essential for successful fracture healing. A thorough validation of results at the precision level required for accurate IFM measurement has not been extensively conducted in past studies. This paper aims to demonstrate through experimental and theoretical investigations that camera-based systems can be used to measure six degrees of freedom micromovements with sufficient accuracy. A pilot study using a micrometre stage evaluated the ability of Vicon, Alvium, and Canon cameras to measure displacements in 0.05 mm increments. Additionally, the effects of marker size, displacement direction, and camera-to-marker distance on measurement accuracy were examined. The rotational capability of the optical systems was also assessed using the law of propagation of uncertainty for uncorrelated quantities and validated through Monte Carlo simulations. For Vicon cameras, the close camera setup yielded more precise measurements than the standard configuration, with maximum marker error values of  $19.1 \pm 11.3 \mu\text{m}$  and  $18.7 \pm 37.0 \mu\text{m}$ , respectively. For the same marker size (14 mm diameter) and displacement direction (lateral), Alvium cameras demonstrated improved precision compared to Canon cameras, with maximum marker error values of  $8.7 \pm 4.4 \mu\text{m}$  and  $20.7 \pm 4.8 \mu\text{m}$ , respectively. Furthermore, the rotational uncertainty was lower for Alvium cameras across all Euler angles than for the other systems tested. These findings lay the groundwork for future studies on IFM measurement and demonstrate that Alvium cameras, when carefully calibrated, can provide accurate IFM measurements in clinical settings.*

**Additional keywords:** Optical tracking, accuracy assessment, laboratory study, analytical study, Interfragment motion

## Abbreviations

Disp	Displacement
DoF	Degrees of freedom
DSLR	Digital single lens reflex
HMA	Human motion analysis system
IFM	Interfragmentary movement
SV	Stereo vision

## 1 Introduction

Bone fractures pose a significant social and economic burden on society [1]. These injuries can cause a decrease in quality of life, job loss, high medical expenses, and extended disability [2, 3]. The situation worsens when the bone fails to heal

properly [2]. Despite advances in fracture treatment, the risk of non-union remains around 1.9%, and can reach as high as 9.2%, depending on factors like injury severity, age, sex, genetics, and bone location [4, 5, 6]. A crucial aspect of successful fracture treatment is establishing mechanical stability, which is achieved through immobilising the bone fragments [7, 8]. This leads to controlled axial interfragmentary movements (IFM) caused by physiological loading from weight-bearing and dynamization techniques [9, 10].

In vivo measurement of fracture stability is limited to radiological evaluation of the formed callus in the clinical setting [11]. However, such methods do not allow for direct measurement of IFM. To address this, researchers have performed in vitro and animal studies to assess and quantify IFM in trauma fractures. These studies indicate that axial IFM values typically range from 0.02 to 1 mm [12, 13, 14]. In contrast, IFM values in distraction and correctional osteotomies are considerably higher, reaching up to 5 mm, with mean values between 1 and 3 mm [15]. It is important to note that the extent of IFM can vary depending on the fixation method and patient loading conditions. Additionally, besides axial IFM, shear and rotational IFM can also occur at the fracture site. These off-axis displacements can hinder recovery by impairing callus formation, disrupting bone bridging, and increasing fibrous tissue development [11, 14].

Understanding IFM is crucial for evaluating the stability and mechanical condition of the fracture site [16]. However, the type and extent of IFM during key clinical procedures, such as trauma osteogenesis, remain unknown. This is because measuring IFM during standard osteosynthesis is difficult without specialised inserts, which are limited to highly experimental studies [17]. Nonetheless, many researchers have used various experimental methods to measure and quantify IFM. These experiments can be grouped into three main categories. The first involves computational tools. The second employs laboratory analysis, in which in vivo conditions are simulated, and loads are applied to the structure through mechanical testing. The third includes in vivo studies with human participants or animal experiments.

Many researchers use computational tools, such as finite element analysis, to evaluate and analyse IFM [16, 18, 19]. These tools enable the calculation of displacement values throughout the entire bone and fixator structure. The primary challenge in adopting this method in clinical practice is the requirement for 3D computed tomography scans and lengthy simulations caused by large mesh sizes [20]. Simulation times can range from hours to weeks, and achieving convergence

can be challenging for some problems. It has been reported that utilising rigid body models instead of deformable models can reduce element mesh size by over 90%, resulting in shorter computation times without compromising accuracy [6]. However, this reduction is mainly observed on high-end computers (workstations), as convergence times remain high on standard office computers.

Biomechanical experiments with cadavers and bone models remain the gold standard for establishing the ground truth on in vitro primary stability assessment of fracture fixation constructs [2]. By integrating mechanical compression tests with infrared optical motion capture systems, researchers have developed a tool for measuring IFM [21, 22]. The mechanical testing machine applies a load to the specimen while the optical system tracks the position of spherical markers attached to the segments. This allows for the measurement of intersegmental translations and rotations at the fracture site. However, this measurement protocol is expensive and has a low throughput. Additionally, manual loading of the specimen might not accurately mimic loading conditions during the human gait cycle.

In vivo IFM measurement involves experiments with either animal or human participants. Because of their similarities to human bone fracture healing, sheep are often used in experimental fracture models [12, 23]. The process involves creating standardised fracture models by resecting the metatarsus or tibia of a sheep limb [12]. Reflective markers are attached to bone segments using half-pins, and infrared optical systems track their positions to measure IFM [24]. Alternatively, Duda et al. [15] conducted clinical experiments to measure IFM in bone fractures stabilised with Ilizarov circular fixators in patients undergoing corrective or distraction osteotomies. The researchers utilised a stereo vision (SV) system to measure and analyse axial and shear IFM. To the best of the authors' knowledge, the study by Duda et al. [15] is the only one that employed human participants for IFM measurement.

Various methodologies have been employed to evaluate the accuracy of optical systems for measuring IFM in both animal and experimental studies. Ammar et al. [22] used a micrometre to assess the accuracy of an optical system for measuring three degrees of freedom (DoF) IFM in comminuted fractures. They reported mean errors of  $0.03 \pm 0.05$  mm for horizontal

measurements and  $0.08 \pm 0.10$  mm for vertical measurements. These values reflect the average differences between the optical system's measurements and the highly accurate reference values set by the micrometre, with the standard deviations indicating the variability of these errors. However, the micrometre was adjusted with large step sizes of about 0.5 mm, and the error analysis was limited to two directional axes.

Kaspar et al. [24] conducted an animal experiment to evaluate 6 DoF measurements at fracture sites stabilised with angle-stable tibial nailing and standard unreamed tibial nailing using an optical motion capture system. They reported system accuracy values of  $\pm 0.1$  mm for axial displacement and shear (anteroposterior and mediolateral), and  $\pm 0.1^\circ$  for angular displacements (axial torsion, anteroposterior and mediolateral bending angles). However, the methodology used to calculate and verify these accuracy values was not described. Additionally, the standard deviations and confidence intervals were not provided.

Some researchers have reported accuracy values of optical motion capture systems by quoting manufacturer-provided figures [15] or values from previous studies [6]. In both cases, the authors cited system accuracy values of 0.05 mm, but these reports lack methodological transparency, as they do not specify how these values were determined or provide statistical metrics like standard deviations or confidence intervals. Without a detailed description of the measurement process, these values cannot be considered traceable or meaningfully compared with other results. Furthermore, even when an accuracy value includes a standard deviation, it does not constitute a comprehensive estimate of measurement uncertainty. A valid uncertainty assessment must consider all relevant sources of measurement error, including system calibration, environmental factors, data processing (including sub-pixel resolution), and human error. Without such an evaluation, the reported figures risk misinterpretation and are insufficient for validating or benchmarking measurement tools.

Given the small IFM expected in many cases (up to 1 mm in the axial direction and possibly much less in the lateral and anterior directions), and the unknown but small expected rotations, it is critical to evaluate the measurement capability of any system used in such a study. The system must also be capable of measuring normal gait while capturing in vivo IFM measurements to evaluate how walking patterns affect fracture motion. This is why optical systems are so frequently used in these studies. However, none of the studies mentioned here reported an in-depth assessment of the measurement capabilities of the systems used. This paper attempts to bridge this gap for future IFM research by evaluating the capabilities of three camera-based systems for measuring 6 DoF micromotions of similar magnitude to IFM. Specifically, the study sought to answer the following questions:

- How do marker size and camera resolution affect the translational accuracy of various optical motion capture systems in measuring micromotions?
- How do the 3D rotational uncertainties of the stereo vision (SV) system—utilising Canon and Alvium cameras—compare to those of the Vicon human motion analysis (HMA) system?

To answer these questions, a pilot study was conducted to

<sup>a</sup> ORCID 0009-0002-5880-3933. Institute for Biomedical Engineering, Stellenbosch University, South Africa. 28431235@sun.ac.za

<sup>b</sup> ORCID 0009-0002-8361-9193. Department of Mechanical Engineering, Katholieke Universiteit Leuven, Belgium. audric.indekeu@student.kuleuven.be.

<sup>c</sup> ORCID 0000-0002-0567-3373. Division of Orthopaedic Surgery, Department of Surgical Sciences, Stellenbosch University, South Africa. nferreira@sun.ac.za

<sup>d</sup> ORCID 0000-0002-0907-508X. Neuromechanics Unit, Central Analytical Facility, Stellenbosch University, South Africa. oloff@sun.ac.za.

<sup>e</sup> ORCID 0000-0003-1537-215X. Department of Mechanical and Mechatronic Engineering, Stellenbosch University, South Africa. kschreve@sun.ac.za.

evaluate the impact of marker size and camera resolution on the accuracy of two SV systems for measuring micromotions in 0.05 mm increments. Additionally, a similar study was performed with the Vicon HMA system to analyse how varying the marker-to-camera distance affects system accuracy. The measurements were also used to calculate the rotational uncertainties of these systems theoretically. The results are presented, compared with ground truth data, and contrasted with findings from similar experiments in the literature.

The findings of this pilot study will be crucial in our future study, which aims to develop a dataset detailing the influence of different fixator configurations and loading conditions on IFM in bone fractures stabilised by hexapod external fixators. Marker clusters affixed to the half pins connected to each bone segment will be used to track the 6 DoF IFM, as illustrated in figure 1.

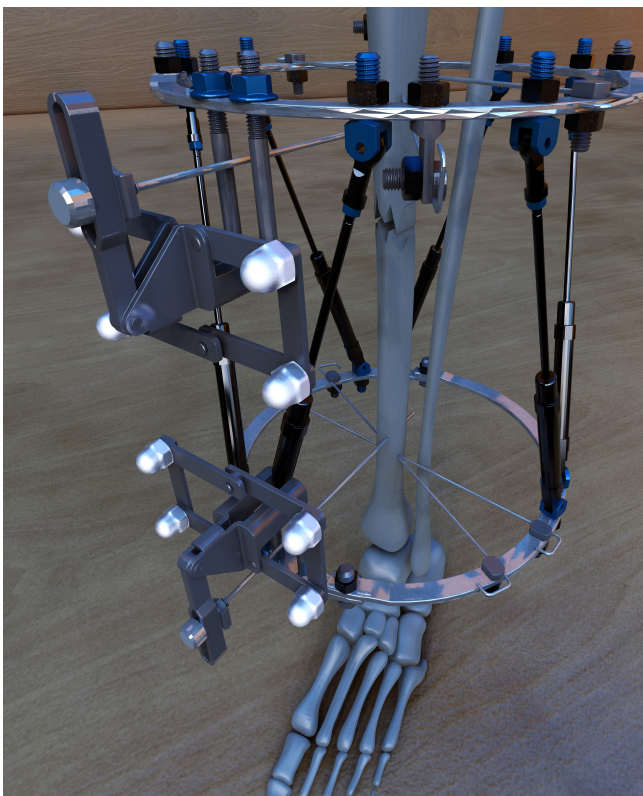


Figure 1 Marker cluster attachment to fixator half pins for IFM measurement

## 2 Materials and Methods

A translational micrometre stage device (Edmund Optics, Barrington, New Jersey, USA) was used to verify the optical systems' ability to measure micromotions in increments of 0.05 mm. According to the conformance certificate, the device has a manufacturer-specified lead screw pitch of 0.5 mm per revolution and a straight-line accuracy of 3  $\mu\text{m}$ . No traceable calibration certificate was available for the product; thus, the measured displacements were based on the manufacturer-specified nominal values.

### 2.1 Data capture with the Vicon HMA system

The study was carried out in the Vicon HMA laboratory within the neuromechanics unit at Stellenbosch University. The lab is equipped with 10 infrared cameras (Vantage V5, Vicon, Oxford, United Kingdom) and 2 video cameras (Bonita 720c, Vicon, Oxford, United Kingdom). The system was calibrated using a Vicon calibration wand (Active Wand V2, Vicon, Oxford Metrics, Oxford, United Kingdom), and the origin was defined at the centre of the capture volume (with the X-axis in the direction of progression, the Z-axis vertical, and the Y-axis to the right).

Prior to data capture, four 14 mm diameter retroreflective markers were securely attached to the moving plate of the micrometre stage. Although three markers were sufficient for motion tracking, a fourth marker was added to improve robustness against potential occlusions and to enable redundancy checks. The device, with the markers mounted, was placed at the centre of the motion capture volume, as shown in figure 2. In addition to the tracking markers, a stationary reference marker was placed near the micrometre stage to evaluate the baseline system noise.

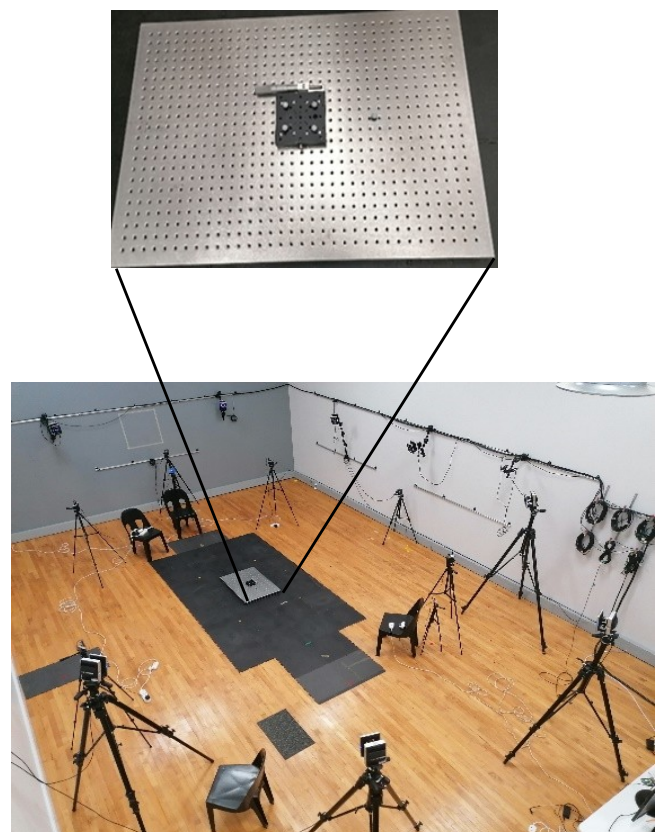


Figure 2 Top: Vicon HMA lab with the micrometre stage in the capture volume; insert: enlarged view of the micrometre stage).

Two experimental sessions were conducted using the Vicon system. During the first session, Vicon cameras were positioned in their standard configuration at a distance of 3000-5000 mm from the micrometre stage. The second session involved a close camera setup, in which two of the furthest 10 Vicon cameras were moved to within 3000 mm of the micrometre stage. This was performed to evaluate the effect of

camera-to-marker distance on measurement accuracy. It is important to note that changing the camera positions requires recalibration before data capture.

The calibrated Vicon system recorded marker positions in the global coordinate system at a frame rate of 200 Hz during each trial. During both sessions, an operator positioned the motion capture volume and adjusted the micrometre stage screw in 0.05 mm increments, covering a total vertical displacement of 1 mm. The operator's position was chosen to ensure that all cameras maintained an unobstructed view of the markers. The system recorded marker trajectories after each vertical adjustment of the plate, but no recording was performed during the application of the incremental step. Thus, each session included 21 incremental adjustments, resulting in a total of 21 trials per session. Marker positions were exported from Vicon Nexus in Excel format. No smoothing filters were applied in Nexus to preserve the raw positional data for analysis.

## 2.2 Data capture with the SV system

In addition to the Vicon HMA system, two SV systems were analysed to assess their ability to measure translational and rotational micromotions. The experiment employed stereo pairs: one with Canon cameras and the other with Alvium cameras; their nominal specifications are listed in table 1.

Table 1 Specifications of Canon and Alvium Cameras

Category	Canon DSLR	Alvium 1800 U
Sensor size	22.3 × 14.9 mm	5.02 × 3.75 mm
Resolution	18 MP	1.6 MP
Pixel size	4.3 × 4.3 μm	3.45 × 3.45 μm
Sensor type	CMOS	CMOS
Dynamic range	11.4 stops	12 stops
Shutter mode	Mechanical shutter	Global shutter

Each pair was mounted at a specific baseline distance to achieve the required epipolar geometry for 3D reconstruction, as shown in figure 3.

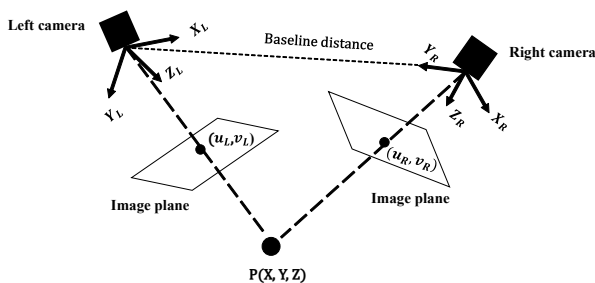


Figure 3 Epipolar geometry

### 2.2.1 Camera calibration

Before each measurement session, the SV systems were calibrated using a calibration plate, depicted in figure 4. The object consists of two planes, XZ and XY. The XZ plane is coplanar with the XZ coordinate plane, while the XY plane

is approximately coplanar with the XY coordinate plane. This configuration enabled the recording of the 3D position of each marker within a volume of 95 × 70 × 70 mm<sup>3</sup>.

Calibration was performed using the RANSAC algorithm as described by Hartley and Zisserman [25]. Two frames of the calibration plate, one from each camera in the pair, were sufficient to calibrate the stereo cameras. The process involved detecting 96 feature points in each image and matching them to their corresponding world points (ground truth) to compute the camera projection matrix and distortion parameters. These parameters were then used to accurately reconstruct the 3D positions of the markers in the scene.

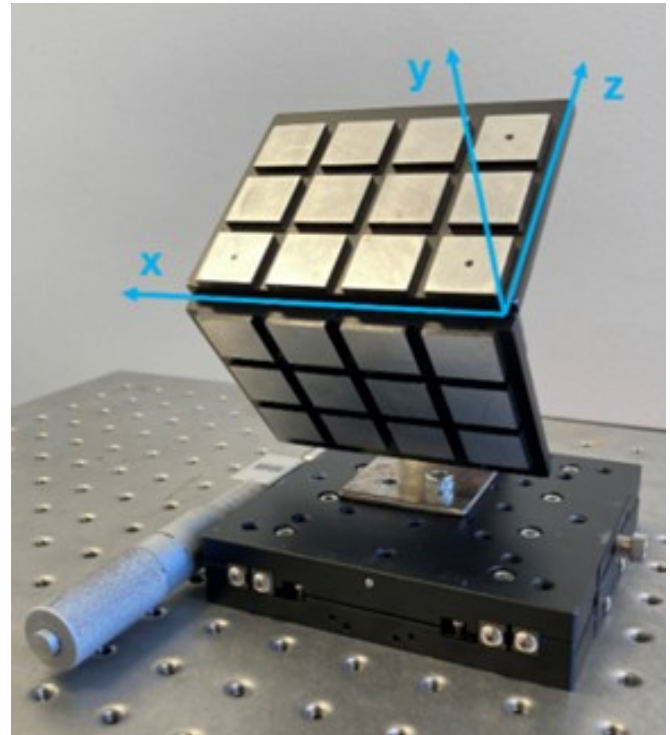


Figure 4 Calibration object with illustration of camera coordinate system

### 2.2.2 Data capture with Canon cameras

The first experiment was conducted using a pair of Canon digital single-lens reflex (DSLR) cameras: EOS 600D and EOS 4000D. The experiment focused on assessing the precision of the Canon cameras in detecting translational micromovements by providing accurate 3D coordinates of objects within the field of view. The cameras were arranged in an epipolar geometry, as shown in figure 6, and captured 72 DPI, 24-bit colour images. They were also set to a 45 mm focal length and an f/18 aperture.

Four printed identical markers were mounted on a movable plate of the micrometre stage. The markers were spaced 60 mm apart horizontally and 40 mm apart vertically. This setup ensured that all markers remained within the calibrated capture volume during testing. The micrometre stage, with the attached markers, was subsequently positioned within the calibrated volume at a distance of 456 mm from the camera lenses, which were separated by a baseline distance of 275 mm.

Three trials were conducted using markers of different

sizes, categorised as big (22 mm diameter), medium (14 mm diameter), and small (9 mm diameter). Data was captured in two controlled directions: first, the plate moved laterally within the camera's field of view, and then it moved axially towards the camera. In both instances, the plate moved in 0.05 mm increments over a total distance of 1 mm. The images were captured remotely to minimise measurement noise caused by slight camera motion.

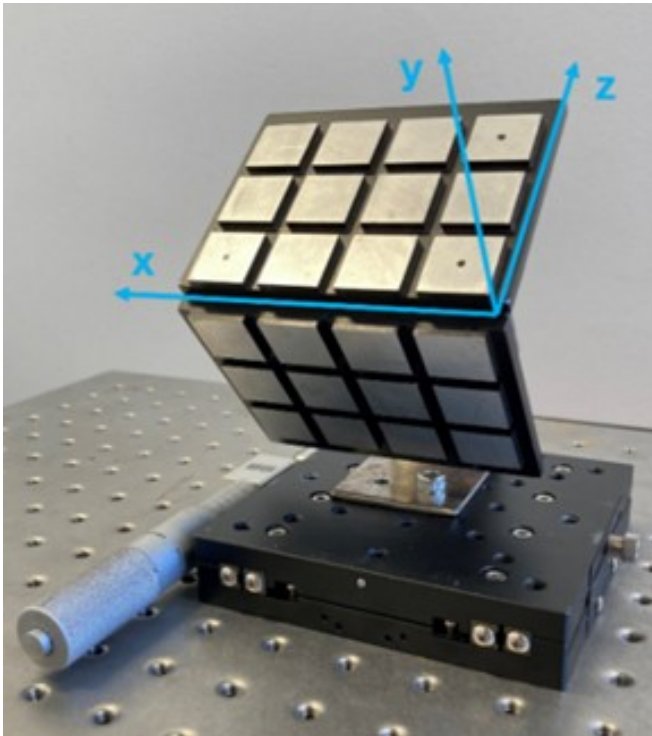


Figure 5 Canon stereo camera setup for marker triangulation

### 2.2.3 Data capture with Alvium cameras

The second experiment was performed using Alvium 1800 U-158 m mono CS-mount cameras. The cameras were set up in the same configuration as Canon cameras and produced 96 DPI, 8-bit grayscale images. They were configured with a 45 mm focal length and an f/18 aperture.

Four big markers (22 mm in diameter) were attached to the moving plate of the micrometre stage, with the marker-to-marker spacing identical to that used in the Canon camera experiment. However, unlike the Canon experiment, the object was positioned 529 mm from the camera lenses, which were spaced 315 mm apart, as shown in Figure 6. According to Ezebebili and Schreve [26], a 73 mm difference in object-to-camera distance is associated with a depth error of 0.285 mm for the furthest point on the object. Moreover, the use of high baseline and focal distances in both stereo camera setups significantly minimises the associated depth errors in 3D reconstruction [27]. Thus, differences in the geometric separation between the camera lenses and the object positions in the two stereo cameras have a negligible effect on the observed results.

Lateral marker displacement in the cameras' viewing plane was examined. This experiment was repeated to evaluate the repeatability of the camera system. As in the previous experiments, the plate moved in increments of 0.05 mm to obtain a

set of 21 frames spanning 1 mm.

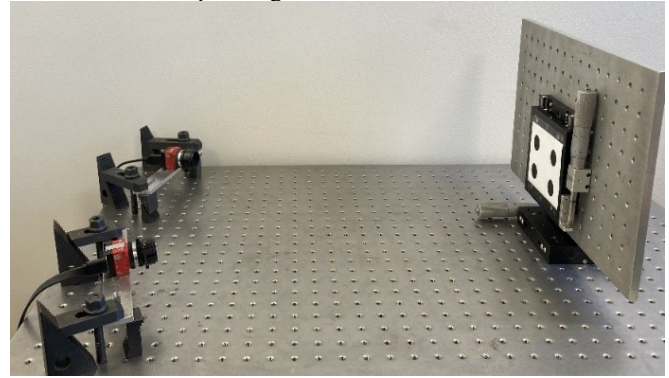


Figure 6 Alvium stereo camera setup for marker triangulation

## 2.3 Data processing

For the SV system, markers from the image planes were extracted as ellipses using an ellipse detection algorithm (OpenCV). The resulting ellipses were utilised to pinpoint the centre of markers with sub-pixel accuracy. The implementation of functional triangulation for each of the extracted 2D centre points within each pair of the captured image frames resulted in the identification of the corresponding 3D coordinates of the markers within the epipolar plane [25]. For the Vicon HMA system, markers were extracted and processed using the built-in pipelines.

The raw data obtained by the Vicon HMA were processed with a moving-average filter to minimise measurement noise. A window size of 10, corresponding to 0.05 s of recording, was selected, as it effectively suppressed noise while minimising excessive data smoothing. On the other hand, static images from the SV system did not require a moving-average filter.

The translational displacement of each marker was analysed by computing the Euclidean distances between the recorded positions across trials. Additionally, error analysis was performed using Monte Carlo simulations, computing the mean absolute difference between the actual displacement reported by the micrometre stage and the displacement measured by both optical systems. These mathematical operations were performed for all trials within each recorded session. It is important to note that the Vicon data from the first trial of the first session were excluded from analysis due to excessive noise, which introduced significant errors in the calculated displacement values. This was observed by the positional measurement of the redundant stationary marker in the scene, which emphasised the valuable utility of such redundant markers.

Ideally, for IFM studies, 6 DoF motion of the bone fragments should be considered, comprising three translations and three rotations. The Vicon HMA and SV systems are capable of measuring 3D translation and 3D rotation. However, since the micrometre stage device was only capable of introducing pure translation displacements, rotation angles were not experimentally recorded. To evaluate the rotational capabilities of both systems for IFM measurement, a theoretical approach was utilised to estimate the uncertainty of the rotational angle

measurements. This was implemented by applying the law of propagation of uncertainty for uncorrelated quantities [28] using equation 1.

$$s_c^2(y) = \sum_{i=1}^N \left( \frac{\partial f}{\partial x_i} \right)^2 s^2(\bar{x}_i) \quad (1)$$

Where  $s_c^2(y)$  is the combined uncertainty of the output quantity,  $s^2(\bar{x}_i)$  is standard variance of the input variable and  $f$  is the relationship between the output and input quantities.

To determine the plate's rotation during translational movements, three points per frame were selected. For the SV system, these points were the centres of the top left, top right, and bottom left markers or  $p_1$ ,  $p_2$  and  $p_3$ , respectively, as depicted in figure 7. For the Vicon data, the points are the centres of the front left, front right, and back left markers.

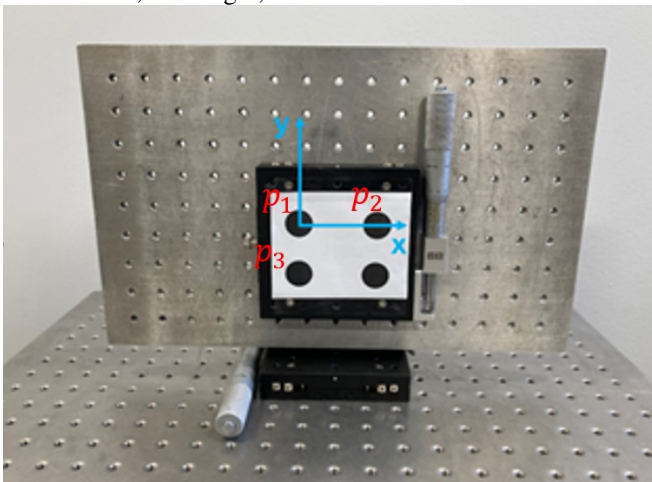


Figure 7 New coordinate system for determining the rotational angles

The angles were calculated from two unit vectors,  $s$  and  $t$ , where:

$$s = \frac{p_2 - p_1}{\|p_2 - p_1\|} \quad (2)$$

and

$$t = \frac{p_3 - p_1}{\|p_3 - p_1\|} \quad (3)$$

A matrix  $M$  can then be defined such that

$$M = \begin{bmatrix} s & t & \frac{s \otimes t}{\|s \otimes t\|} \end{bmatrix} \quad (4)$$

defines a coordinate frame. To facilitate comparisons with previous studies, which often report only mean values and standard deviations without a full uncertainty analysis, it was assumed that the vectors  $s$  and  $t$  are perpendicular, thereby simplifying the uncertainty analysis.  $M$  depends entirely on the 3D coordinates determined from the initial position of the markers. A similar matrix  $N$  can be defined for the coordinates of the rotated markers' positions and is given by:

$$N = \begin{bmatrix} s' & t' & \frac{s' \otimes t'}{\|s' \otimes t'\|} \end{bmatrix} \quad (5)$$

Thus, the rotation between the two coordinate frames can be defined as follows:

$$R = NM^T \quad (6)$$

The three Euler angles (yaw, pitch and roll) can be determined from the following:

$$f_{yaw} = \arctan \frac{R_{2,1}}{R_{1,1}} \quad (7)$$

$$f_{pitch} = \arctan \frac{R_{3,1}}{R_{1,1} \cos(f_{yaw}) + R_{2,1} \sin(f_{yaw})} \quad (8)$$

$$f_{roll} = \arctan \frac{R_{3,2}}{R_{3,3}} \quad (9)$$

Where  $R_{i,j}$  refers to the element in the rotation matrix at row  $i$  and column  $j$ . Thus, the function  $f$  representing roll, yaw, and pitch depends on 18 variables: the 3D coordinates of the three selected markers at both the initial and rotated positions. The resulting rotations are described relative to the global reference system.

The analytical approach assumes that input uncertainties are uncorrelated and that the function can be linearised around the mean (valid for small angles but not for large ones) [28]. These assumptions can sometimes produce unrealistic uncertainty estimates. To address these limitations and improve accuracy, Monte Carlo simulations were employed as a supplementary method, owing to their ability to handle non-linear functions and correlated input uncertainties. The uncertainties of the respective Euler angles were calculated by incorporating equations (2) through (9) into the simulations. A total of 100000 iterations were performed.

### 3 Results

#### 3.1 Displacement results for the Canon SV system

Figures 8 and 9 show the results of lateral and axial displacement for three different marker sizes as recorded by Canon stereo cameras. There is a strong correlation between the measured values and the ground truth data. However, the most accurate results were obtained for the medium markers in the lateral direction.

Table 2 presents the mean values of the absolute difference between the measured and actual displacement for all marker sizes. The medium markers exhibit mean values of less than  $9 \mu\text{m}$  and  $23 \mu\text{m}$  in the lateral and axial directions, respectively. The small markers gave less accurate results, with mean values ranging from  $12$  to  $55 \mu\text{m}$ , while the big markers ranged from  $6$  to  $50 \mu\text{m}$ . An important observation is the effect of the displacement's direction on measurement accuracy. As expected, displacements in the lateral direction were more accurate than displacements in the axial direction.

#### 3.2 Displacements results for Alvim SV system

Figure 10 presents the displacement results for the two sessions recorded by the Alvim cameras using large markers. The displacement occurred laterally in both sessions. There is a strong correlation between the measured points and the

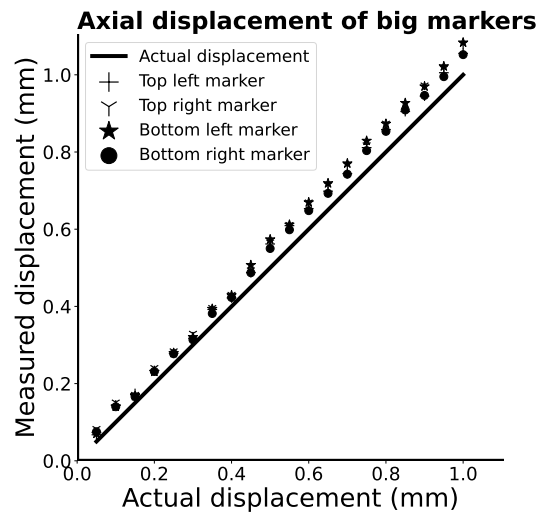
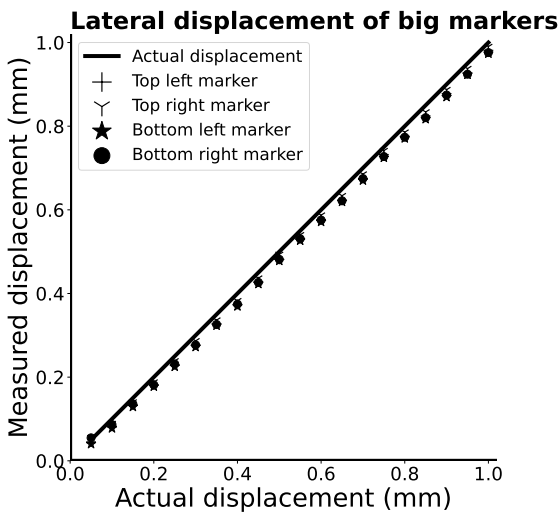
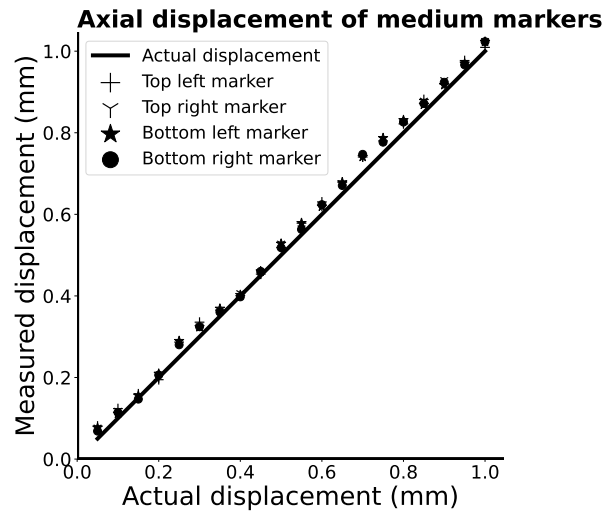
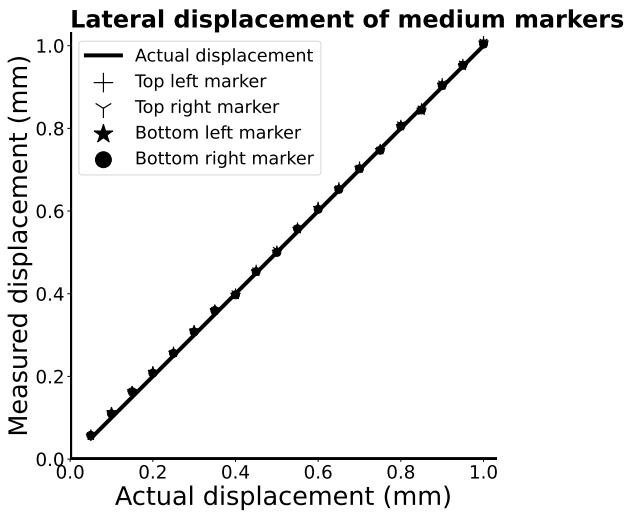
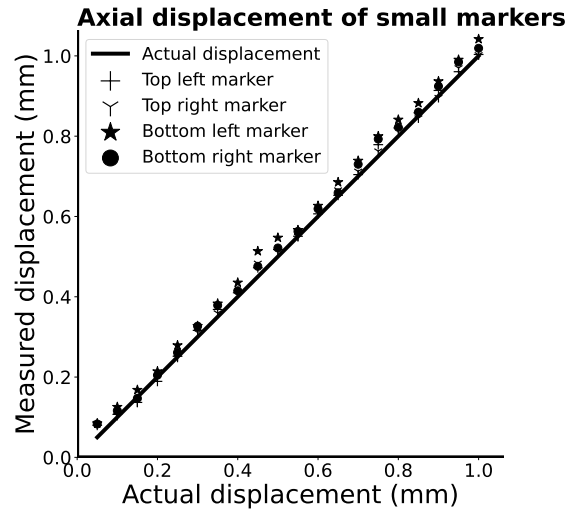
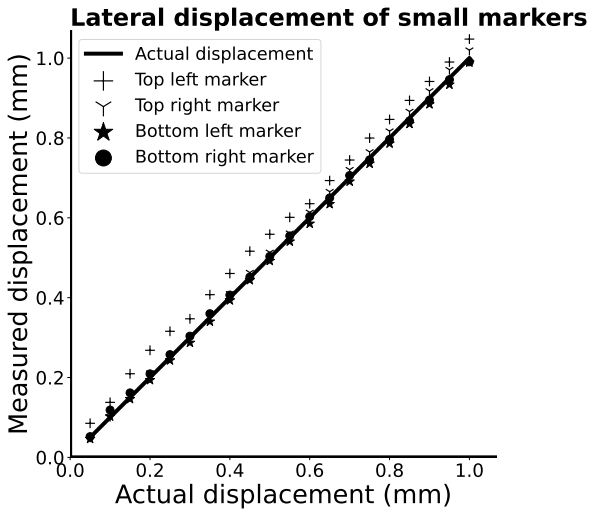


Figure 8 Measured vs actual total displacement (Canon stereo cameras) - lateral view

Figure 9 Measured vs actual total displacement (Canon stereo cameras) - axial view

Table 2 Displacement error values for SV system,  $\sigma$  denotes uncertainty and disp represents displacement.

Marker size	Position	Lateral disp mean $\pm\sigma$ ( $\mu\text{m}$ )	Axial disp mean $\pm\sigma$ ( $\mu\text{m}$ )
Big	Top left	20.72 $\pm$ 4.78	43.27 $\pm$ 14.48
	Top right	11.96 $\pm$ 3.09	54.72 $\pm$ 17.62
	Bottom left	25.88 $\pm$ 4.90	54.35 $\pm$ 22.16
	Bottom right	21.72 $\pm$ 5.73	39.40 $\pm$ 12.78
Medium	Top left	8.80 $\pm$ 4.05	22.41 $\pm$ 11.38
	Top right	7.37 $\pm$ 3.16	21.51 $\pm$ 11.02
	Bottom left	6.44 $\pm$ 3.69	21.97 $\pm$ 10.62
	Bottom right	5.33 $\pm$ 3.06	19.02 $\pm$ 10.14
Small	Top left	50.00 $\pm$ 10.17	12.35 $\pm$ 8.37
	Top right	12.00 $\pm$ 6.05	11.726 $\pm$ 9.33
	Bottom left	9.97 $\pm$ 4.32	34.32 $\pm$ 11.54
	Bottom right	20.48 $\pm$ 4.08	20.48 $\pm$ 10.27

ground truth data. Additionally, the findings are repeatable, as similar results were obtained when the experiment was re-taken.

Table 3 shows the mean values of the absolute difference between the measured and actual displacement for data recorded by the Alvium cameras. The values were smaller than 9  $\mu\text{m}$  and 5  $\mu\text{m}$  for the first and second sessions, respectively.

These outcomes are promising compared to the data recorded by the Canon cameras for the same marker sizes. This clearly shows that the displacement values measured with the Alvium cameras are more precise than those measured with Canon cameras.

Table 3 Displacement error for Alvium SV system,  $\sigma$  denotes uncertainty.

Marker	Session 1 mean $\pm\sigma$ ( $\mu\text{m}$ )	Session 2 mean $\pm\sigma$ ( $\mu\text{m}$ )
Top left	6.73 $\pm$ 4.29	4.62 $\pm$ 2.96
Top right	8.736 $\pm$ 4.42	2.91 $\pm$ 2.02
Bottom left	3.66 $\pm$ 2.35	2.03 $\pm$ 1.16
Bottom right	5.78 $\pm$ 3.14	2.13 $\pm$ 1.34

### 3.3 Displacements results for the Vicon HMA system

As mentioned, two sessions were conducted with the Vicon motion HMA system. The results for both sessions show a high correlation between the actual and measured values, as illustrated in figure 11. However, in the first session, there is a notable discrepancy between some measured points and the actual displacement values, which is also apparent in the reference marker's displacement values. Convergence is significantly improved in the second session, with most data points closely aligned with the actual displacement values.

Table 4 shows the discrepancy between the actual and the measured displacement values for corresponding marker positions. The values are higher during the second session, reaching 19.10  $\mu\text{m}$ , compared to the first session, which reaches 16.06  $\mu\text{m}$ . However, the uncertainties are higher in the first session, reaching 39.50  $\mu\text{m}$ , compared to the second session,

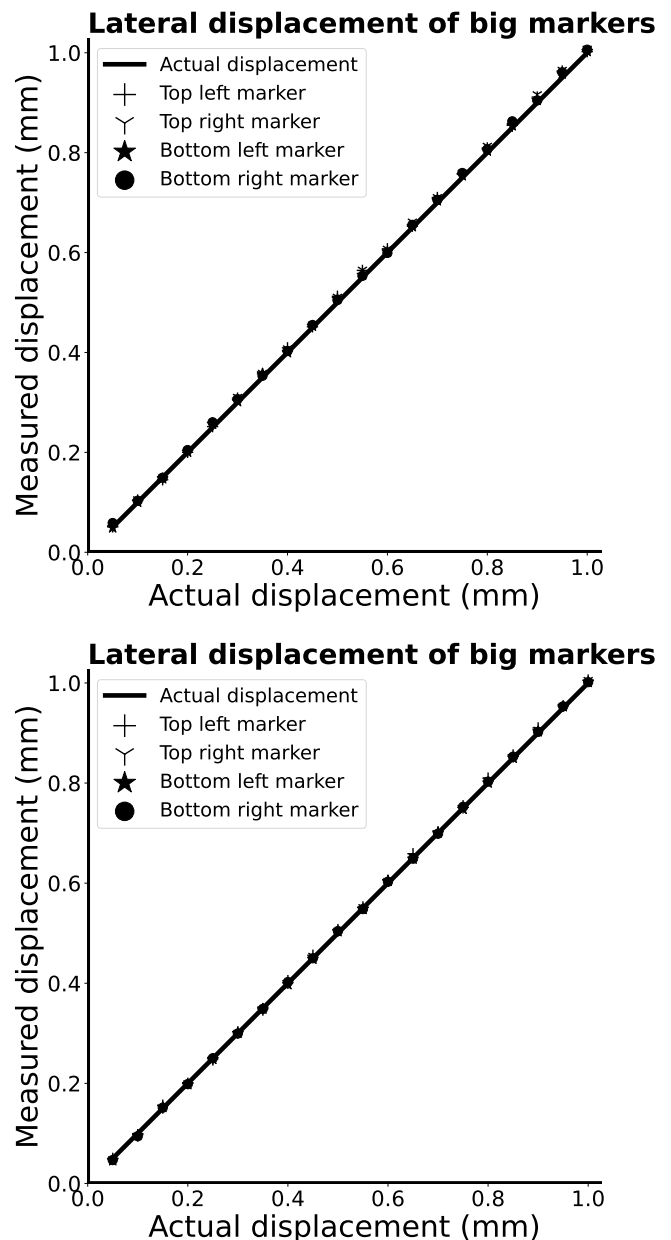


Figure 10 Measured vs actual total displacement (Alvium SV system): Top: session 1, bottom: session 2

which reaches 11.60  $\mu\text{m}$ . This clearly demonstrates that the measurement precision improves with a closer camera setup than the standard configuration.

To gain further insights into the uncertainty of the measurements, linear regression lines were fitted using the least squares method [29]. For each marker, 20-point distances were utilised to come up with the regression line and the 95% prediction interval for both the SV and Vicon data, as shown in figure 12.

For the Vicon data, point distances for all four markers recorded during the second session were used to generate the regression line. The first session data was excluded from the analysis due to high measurement noise. For the stereo vision data, only the medium bottom right marker was used to generate the regression line. Although the graphs for the other marker sizes appeared similar, the data for the small and large markers showed noticeable deviations between the actual dis-

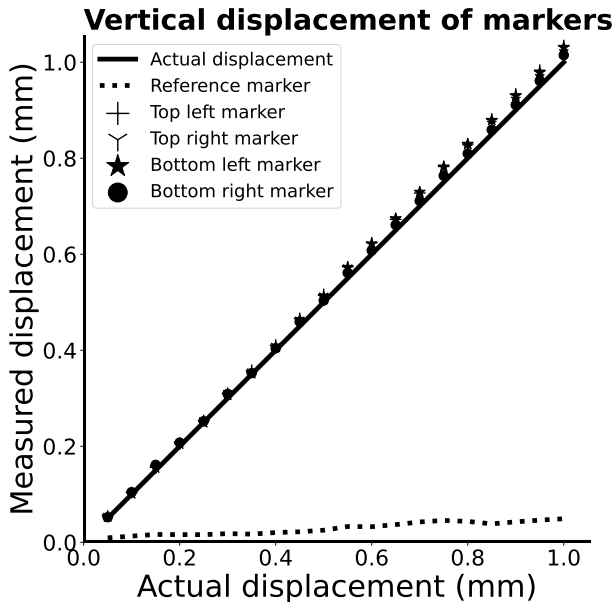
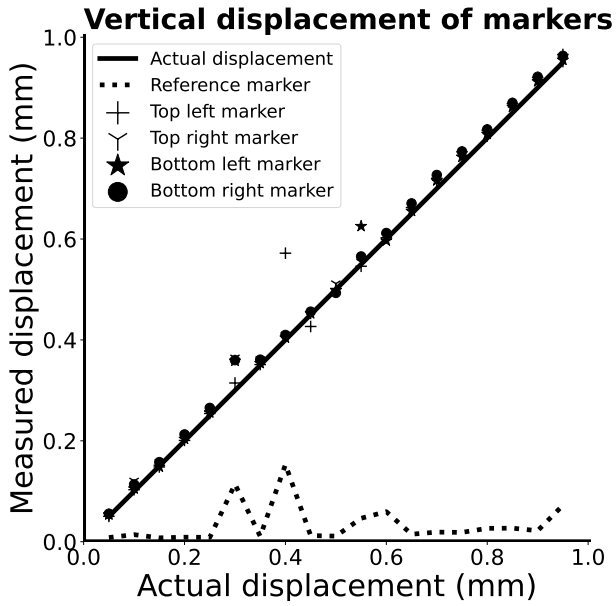


Figure 11 Measured vs actual total displacement (Vicon HMA system): Top: session 1, bottom: session 2

placement and the linear regression lines. Overall, the linear regression line aligned with the actual displacement line for the selected datasets, indicating that the measurements were accurate.

To determine the uncertainty of total displacement, the maximum difference between the linear regression line and the 95% prediction interval was selected. This indicates the worst-case prediction uncertainty for the total displacements for both the SV and Vicon cameras. These values were used as the upper bounds for coordinate uncertainty. When calculating the uncertainty of individual coordinates using the analytical method, it was assumed that the uncertainty was the same for all three coordinates. This assumption was not necessary for the Monte Carlo simulation method, which distributes

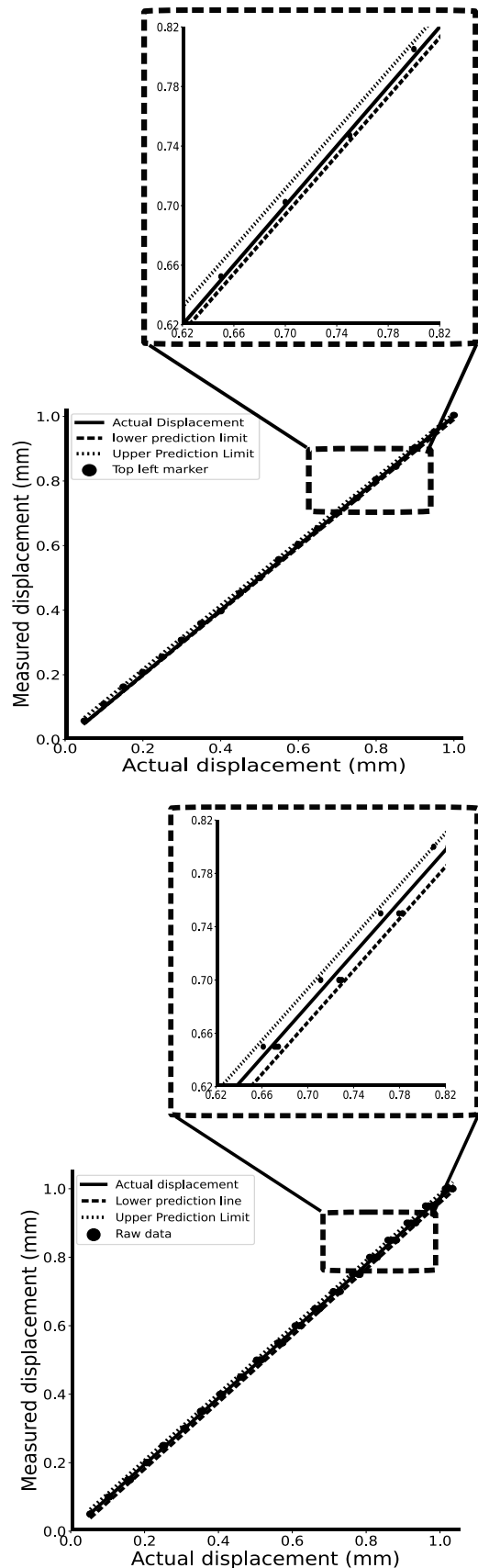


Figure 12 95% prediction intervals: Top: SV data, bottom: Vicon data.

Table 4 Displacement error for Vicon HMA system,  $\sigma$  denotes uncertainty.

Marker	Session 1 mean $\pm\sigma$ ( $\mu\text{m}$ )	Session 2 mean $\pm\sigma$ ( $\mu\text{m}$ )
Top left	18.74 $\pm$ 37.03	19.05 $\pm$ 11.30
Top right	11.25 $\pm$ 13.32	14.95 $\pm$ 8.23
Bottom left	12.65 $\pm$ 19.24	16.75 $\pm$ 11.77
Bottom right	16.78 $\pm$ 11.75	8.40 $\pm$ 3.78

uncertainty values unevenly among the coordinates based on the geometry of the displacement line.

Table 5 shows the uncertainty of the individual coordinates as derived from the uncertainty of the total displacement using both the law of propagation of uncertainty for uncorrelated quantities and the Monte Carlo simulations.

Table 5 Uncertainty of individual coordinates ( $\sigma_{\text{coords}}$ ) derived from the uncertainty of total displacement ( $\sigma_{\text{disp}}$ ).

Camera system	$\sigma_{\text{disp}}$	LPUUQ	MCS
		[ $\sigma_{\text{coords}}$ ( $\mu\text{m}$ )]	[ $\sigma_{\text{coords}}$ ( $\mu\text{m}$ )]
Canon	29.48	20.84	(18.64, 26.6, 12.93)
Alvium	10.44	7.38	(0.56, 7.99, 6.74)
Vicon	12.95	9.16	(4.00, 7.83, 9.59)

**Note:** LPUUQ stands for the law of propagation of uncertainty for uncorrelated quantities; MCS refers to Monte Carlo simulations

The uncertainties for the different Euler angles were calculated using the arctangent function  $f$  together with the 18 coordinate variables. The results are shown in table 6. Three sets of coordinates were tested at each angle, and the maximum values were recorded.

Table 6 Maximum uncertainty of rotation for the roll-pitch-yaw angles

Camera system	Roll ( $^{\circ}$ )	Pitch ( $^{\circ}$ )	Yaw ( $^{\circ}$ )
Canon	0.059 (0.057)	0.044 (0.024)	0.046 (0.049)
Alvium	0.021 (0.020)	0.016 (0.012)	0.016 (0.015)
Vicon	0.026 (0.015)	0.019 (0.020)	0.019 (0.016)

**Note.** Values outside brackets represent uncertainties obtained using the analytical method; those within brackets denote uncertainties obtained using the Monte Carlo simulation method.

## 4 Discussion

The pilot study aimed to investigate the effectiveness of the Vicon HMA and SV systems in detecting micromotions of similar magnitude to IFM. Displacements of 0.05 mm were applied in increments, totalling 1 mm, using the micrometre stage. For both systems, the results reveal a strong correlation between the measured and actual displacement values. This is supported by the observed low maximum absolute mean difference values of 19  $\mu\text{m}$ , 50  $\mu\text{m}$ , and 7  $\mu\text{m}$  for the Vicon, Canon and Alvium cameras, respectively. Furthermore, the study analysed the influence of camera setup, camera resolution, and marker size on measurement accuracy.

Despite the Vicon HMA system registering low error values, the standard configuration (far camera setup) was observed to produce more measurement noise than the close camera setup. These unusual displacements aligned with the

reference (stationary) marker, suggesting that motion artefacts from investigator movement in the laboratory may have affected this session. For points outside the heavily noise-affected regions, the displacement measurements are closely aligned with the ground truth data, as shown in figure 10. The results might have improved, as with the close camera setup, if the session had been repeated under conditions with minimal movement in the lab. However, this test demonstrated the efficacy of having such redundant markers, which enhance the evaluation of measurement confidence.

Marker size and displacement direction have been observed to influence the accuracy of the SV system in measuring micromotion. The results depicted in figure 7 show that medium markers are associated with more accurate results than the other markers used in the study. Thus, it can be inferred that there is a limit to the size of markers that improve measurement accuracy, with 14 mm-diameter markers being the most effective among those tested in this study. This is justified, as large markers, despite their higher pixel count, are more prone to optical blurring and distortions [30].

Regarding displacement direction, lateral movements produced more accurate results than axial movements for both markers. This is quite understandable as SV systems exhibit larger depth errors than lateral errors [31]. Since controlled lateral displacements were applied in the study, marker depth remained constant, thereby improving lateral accuracy. However, in clinical settings, lateral movements are often accompanied by depth changes, which can reduce the measurement accuracy.

A strong correlation was observed between the measured values and the ground truth data for the SV system using Alvium cameras. These results far exceed those obtained with Canon cameras for the same capture volume and marker size. Despite having lower nominal specifications than Canon cameras (table1), Alvium cameras employ monochrome sensors, in which all the incoming light is captured at each pixel. In contrast, Canon cameras utilise colour sensors, where each pixel records only one primary colour, while the other components are interpolated from neighbouring pixels through demosaicing [32]. Interpolation modifies the recorded pixel intensities, as each final value is the weighted average of its neighbours [33]. This could reduce the accuracy of marker detection and tracking. Moreover, differences in lens and processor quality could also contribute to the variations in the results.

The rotation uncertainties were derived theoretically from the uncertainties in the marker's 3D coordinates. Similar results were observed for most Euler angles when comparing the analytical method with Monte Carlo simulations, although the latter yielded relatively smaller uncertainty values (figure 5). This demonstrates the validity of the analytical approach for estimating rotational uncertainties, particularly for small angular displacements. However, validation with Monte Carlo simulations is recommended when dealing with correlated input quantities or large angular displacements.

Canon cameras produced uncertainty values of not more than 0.022 mm in translation and 0.059 $^{\circ}$  in rotation, while the Vicon cameras achieved values below 0.037 mm in translation and 0.026 $^{\circ}$  in rotation. Alvium cameras provided even

more precise measurements with uncertainty values below 0.004 mm in translation and  $0.021^\circ$  in rotation. This suggests that Alvium cameras are better suited for measuring 6 DoF micromotion compared to the other optical systems tested in this study. However, it is essential to note that the uncertainty values for all the tested camera systems are comparable to, or even better than, the accuracy values reported in the literature, where translational and rotational accuracy values of 0.05 mm and  $0.1^\circ$ , respectively, have been documented [6, 15].

The interpretation of the 3D rotation uncertainty leads to interesting conclusions. The cameras exhibit the poorest visibility in detecting rotation around the x-axis, as illustrated in table 5. This is expected, as SV cameras are less sensitive to lateral movements, which do not significantly impact depth perception (the relative position of the markers to the cameras). Consequently, the cameras are more effective at detecting rotations around the other two axes. Similar results were observed with the Vicon cameras, where the uncertainty value was relatively high for rotations around the x-axis. It is important to emphasise that these theoretical uncertainty values represent the conservative limits for both types of camera systems, and the actual uncertainty values are likely to be lower. Additionally, these calculations were based on three of the four markers for each frame. Including the fourth marker in the calculation would likely yield even more accurate results.

The uncertainty values reported here will help future IFM studies determine the limitations of achievable measurements. It will also give confidence in the results. From these experiments, the value of redundant markers was highlighted, as they help assess whether the results of a trial can be trusted. The results also show that an independent, close-up SV system will yield the most accurate IFM results, and these results can be supported with measurements from the Vicon system (or a similar system) to obtain the full gait results.

## 5 Study Limitations

The primary limitation of this study is that only translational motions were measured. A comprehensive validation should have included angular displacements, as the envisioned research aims to measure the 6 DoF IFM. However, the theoretical uncertainty values still provide insights into the capability of the three optical systems to measure angular displacements. Another limitation is that only a single trial was conducted with the Vicon cameras. Multiple trials would have helped assess the system's repeatability for micromotion measurements. Finally, the measured parameters are not traceable to any international standard due to the lack of a calibration certificate for the micrometre stage and also the absence of certified laboratories for validation.

## 6 Conclusion

The Vicon HMA and SV systems (utilising both Canon and Alvium cameras) are capable of measuring 6 DoF micromotion with high accuracy. By triangulating 2D image coordinates, the system accurately reconstructed the 3D coordinates of markers. Minimal discrepancies and uncertainties were observed compared with ground truth data. However, Alvium

cameras demonstrated superior performance relative to the other camera systems. Furthermore, there is a limit to the size of markers that improves tracking with 14 mm diameter markers, demonstrating better performance among the tested options.

The study's findings will be crucial in our envisioned research, which aims to develop a dataset detailing the influence of the hexapod external fixator's configuration and patient loading conditions on IFM. Additionally, these results will provide other researchers investigating IFM with confidence in the accuracy of their findings and help them identify the limitations of the measurements. By integrating SV cameras with the Vicon system, complete gait data can be collected, enabling a more thorough assessment of the influence of biomechanical parameters on IFM.

## References

- [1] Russel Burge, Bess Dawson-Hughes, Daniel H Solomon, John B Wong, Alison King, and Anna Tosteson. Incidence and economic burden of osteoporosis-related fractures in the united states, 2005–2025. *Journal of bone and mineral research*, 22(3):465–475, 2007.
- [2] Gregory S Lewis, Dominic Mischler, Hwabok Wee, J Spence Reid, and Peter Varga. Finite element analysis of fracture fixation. *Current osteoporosis reports*, 19(4):403–416, 2021.
- [3] Jens Christian Richter, Christian Waydhas, and Frank-Gerald Pajonk. Incidence of posttraumatic stress disorder after prolonged surgical intensive care unit treatment. *Psychosomatics*, 47(3):223–230, 2006.
- [4] Julius A Bishop, Ariel A Palanca, Michael J Bellino, and David W Lowenberg. Assessment of compromised fracture healing. *JAAOS-Journal of the American Academy of Orthopaedic Surgeons*, 20(5):273–282, 2012.
- [5] Leanora A Mills, Stuart A Aitken, and A Hamish RW Simpson. The risk of non-union per fracture: current myths and revised figures from a population of over 4 million adults. *Acta orthopaedica*, 88(4):434–439, 2017.
- [6] Mischa Mühling, M Winkler, and Peter Augat. Prediction of interfragmentary movement in fracture fixation constructs using a combination of finite element modeling and rigid body assumptions. *Computer Methods in Biomechanics and Biomedical Engineering*, 24(15):1752–1760, 2021.
- [7] Peter Augat, Marianne Hollensteiner, and Christian von Rüden. The role of mechanical stimulation in the enhancement of bone healing. *Injury*, 52:S78–S83, 2021.
- [8] Hans K Uthoff, Philippe Poitras, and David S Backman. Internal plate fixation of fractures: short history and recent developments. *Journal of Orthopaedic Science*, 11(2):118–126, 2006.

- [9] Tianyong Hou, Qiang Li, Fei Luo, Jianzhong Xu, Zhao Xie, Xuehui Wu, and Chengling Zhu. Controlled dynamization to enhance reconstruction capacity of tissue-engineered bone in healing critically sized bone defects: an in vivo study in goats. *Tissue Engineering Part A*, 16(1):201–212, 2010.
- [10] Saeed Miramini, Lihai Zhang, Martin Richardson, Marinis Pirpiris, Priyan Mendis, Kunle Oloyede, and Glenn Edwards. Computational simulation of the early stage of bone healing under different configurations of locking compression plates. *Computer methods in biomechanics and biomedical engineering*, 18(8):900–913, 2015.
- [11] Peter Augat, Johannes Burger, Sandra Schorlemmer, Thomas Henke, Manfred Peraus, and Lutz Claes. Shear movement at the fracture site delays healing in a diaphyseal fracture model. *Journal of orthopaedic research*, 21(6):1011–1017, 2003.
- [12] Lutz E Claes, Christa A Heigele, Cornelia Neidlinger-Wilke, Daniela Kaspar, Walter Seidl, Kristen J Margevicius, and Peter Augat. Effects of mechanical factors on the fracture healing process. *Clinical Orthopaedics and Related Research (1976-2007)*, 355:S132–S147, 1998.
- [13] S Wolf, A Janousek, J Pfeil, W Veith, F Haas, G Duda, and L Claes. The effects of external mechanical stimulation on the healing of diaphyseal osteotomies fixed by flexible external fixation. *Clinical biomechanics*, 13(4-5):359–364, 1998.
- [14] Devakara R Epari, William R Taylor, Markus O Heller, and Georg N Duda. Mechanical conditions in the initial phase of bone healing. *Clinical biomechanics*, 21(6):646–655, 2006.
- [15] Georg N Duda, Simon Sporrer, Michael Sollmann, Jan E Hoffmann, Jean-Pierre Kassi, Cyrus Khodadadyan, and Michael Raschke. Interfragmentary movements in the early phase of healing in distraction and correction osteotomies stabilized with ring fixators. *Langenbeck's Archives of Surgery*, 387(11):433–440, 2003.
- [16] GN Duda, JP Kassi, JE Hoffmann, R Riedt, C Khodadadyan, and M Raschke. Mechanical behavior of ilizarov ring fixators. effect of frame parameters on stiffness and consequences for clinical use. *Der Unfallchirurg*, 103(10):839–845, 2000.
- [17] Benedikt J Braun, Tim Pohlemann, Steven C Herath, Moritz Klein, Mika F Rollmann, Ralf Derr, Stefan Diebels, and Michael Roland. An individualized simulation model based on continuous, independent, ground force measurements after intramedullary stabilization of a tibia fracture. *Archive of Applied Mechanics*, 89(11):2351–2360, 2019.
- [18] Farhad Nabhani, Edward J Bradley, and Simon Hodgson. Comparison of two tools for the measurement of interfragmentary movement in femoral neck fractures stabilised by cannulated screws. *Robotics and Computer-Integrated Manufacturing*, 26(6):610–615, 2010.
- [19] Peter Augat, M Faschingbauer, K Seide, K Tobita, SA Callary, LB Solomon, and JH Holstein. Biomechanical methods for the assessment of fracture repair. *Injury*, 45:S32–S38, 2014.
- [20] Ihor Farmaga, Petro Shmigelskyi, Piotr Spiewak, and Lukasz Ciupinski. Evaluation of computational complexity of finite element analysis. In *2011 11th International Conference The Experience of Designing and Application of CAD Systems in Microelectronics (CADSM)*, pages 213–214. IEEE, 2011.
- [21] Stefan Doebele, Sebastian Siebenlist, Helen Vester, Petra Wolf, Ulrich Hagn, Ulrich Schreiber, Ulrich Stöckle, and Martin Lucke. New method for detection of complex 3d fracture motion-verification of an optical motion analysis system for biomechanical studies. *BMC musculoskeletal disorders*, 13(1):33, 2012.
- [22] A Ammar, A Koshyk, M Kohut, B Alolabi, and CE Quenneville. The use of optical tracking to characterize fracture gap motions and estimate healing potential in comminuted biomechanical models of surgical repair. *Annals of Biomedical Engineering*, 51(10):2258–2266, 2023.
- [23] Georg N Duda, Kerstin Eckert-Hübner, Roman Sokiranski, Albert Kreutner, Rudolf Miller, and Lutz Claes. Analysis of inter-fragmentary movement as a function of musculoskeletal loading conditions in sheep. *Journal of biomechanics*, 31(3):201–210, 1997.
- [24] K Kaspar, H Schell, P Seebeck, MS Thompson, Michael Schuetz, NP Haas, and GN Duda. Angle stable locking reduces interfragmentary movements and promotes healing after unreamed nailing: Study of a displaced osteotomy model in sheep tibiae. *JBJS*, 87(9):2028–2037, 2005.
- [25] Richard Hartley and Andrew Zisserman. *Multiple view geometry in computer vision*. Cambridge university press, 2003.
- [26] Ifeanyi F Ezebili and Kristiaan Schreve. Propagation of uncertainty for an epipole-dependent model for convergent stereovision structure computation. *Measurement Science and Technology*, 35(4):045032, 2024.
- [27] David Fernández Llorca, Miguel Ángel Sotelo Vázquez, Ignacio Parra Alonso, Manuel Ocaña Miguel, Luis Miguel Bergasa Pascual, et al. Error analysis in a stereo vision-based pedestrian detection sensor for collision avoidance applications. 2010.
- [28] Jailton Carreteiro Damasceno and PR Couto. *Methods for evaluation of measurement uncertainty*, volume 2. IntechOpen London, UK, 2018.
- [29] Ronald E Walpole, Raymond H Myers, Sharon L Myers, and Keying Ye. *Probability and statistics for engineers and scientists*, volume 5. Macmillan New York, 1993.

- [30] Feng Yan, Zhen Liu, Xiao Pan, and Yuan Shen. High-accuracy calibration of cameras without depth of field and target size limitations. *Optics Express*, 28(19): 27443–27458, 2020.
- [31] Jinglin Peng. *Comparison of three dimensional measurement accuracy using stereo vision*. PhD thesis, Faculty of Graduate Studies and Research, University of Regina, 2011.
- [32] Ala Hijazi, Ahmad Al-Masri, and Nathir Rawashdeh. On the use of bayer sensor color cameras in digital image correlation. In *2022 11th International Symposium on Signal, Image, Video and Communications (ISIVC)*, pages 1–7. IEEE, 2022.
- [33] Bahadir K Gunturk, John Glotzbach, Yucel Altunbasak, Ronald W Schafer, and Russel M Mersereau. Demosaicking: color filter array interpolation. *IEEE Signal processing magazine*, 22(1):44–54, 2005.